Studies of bonding defects, and defect state suppression in HfO2 by soft X-ray absorption and photoelectron spectroscopies

ARTICLE *in* SURFACE SCIENCE · SEPTEMBER 2007

Impact Factor: 1.93 · DOI: 10.1016/j.susc.2007.04.197

6 AUTHORS, INCLUDING:

G. Lucovsky
North Carolina State University
544 PUBLICATIONS **13,360** CITATIONS
SEE PROFILE

Hyungtak Seo
Ajou University
85 PUBLICATIONS **631** CITATIONS
SEE PROFILE

Gennadi Bersuker
Aerospace Corporation
535 PUBLICATIONS **5,304** CITATIONS
SEE PROFILE

Available online at www.sciencedirect.com
ScienceDirect
Surface Science 601 (2007) 4236–4241
SURFACE SCIENCE
www.elsevier.com/locate/susc

Studies of bonding defects, and defect state suppression in HfO_2 by soft X-ray absorption and photoelectron spectroscopies

G. Lucovsky [a,*], H. Seo [a], L.B. Fleming [a], J. Lüning [b], P. Lysaght [c], G. Bersuker [c]

[a] *Department of Physics, NC State University, Raleigh, NC 27695-8202, USA*
[b] *Stanford Synchrotron Radiation Laboratory, Menlo Park, CA 94025, USA*
[c] *Sematech, Austin, TX 78741, USA*

Available online 29 April 2007

Abstract

This paper identifies *two-different regimes* of nano-crystallinity: (i) thin films with nano-crystallites >3 nm, that display coherent well-defined grain-boundaries, and (ii) thin films with nano-crystallites less than ~2 nm, that display neither will-defined grain-boundaries nor lattice planes in high resolution transmission electron microscopy images, but yield an image indicative of clusters of small nano-crystallites with a length scale order of ~2 nm. Near edge X-ray absorption spectroscopy, and soft-X-ray photoelectron spectroscopy, combined with visible and UV spectroscopic ellipsometry, provide an unambiguous way to distinguish between these two *technologically important* regimes of nano-crystalline order, yielding significant information on electronic structure of intrinsic band edge states and intrinsic electronically-active defects.

Keywords: Transition metal oxides; Crystal field and Jahn–Teller d-state splittings; Ab initio molecular orbital theory; Intrinsic bonding states; Intrinsic defect states

1. Introduction

Densities of interfacial and bulk traps in high-κ dielectrics are typically about two orders of magnitude higher ($\sim 10^{12}$ cm^{-2}) than in Si–SiO_2 devices [1]. A crucial issue is to determine whether these high-κ defects are intrinsic and associated with the *microstructure*, nano-crystalline or noncrystalline, or whether they are from process related chemical impurities. Spectroscopic studies of high-κ gate dielectrics are presented with an emphasis on identification of electron and hole traps in gate stacks containing HfO_2 [1–7]. An asymmetry in hole and electron trapping is a potentially significant limitation for the operation and reliability of Si complementary metal oxide semiconductor (CMOS) devices and circuits.

Based on spectroscopic studies and electronic structure calculations, asymmetries in electron and hole trapping were initially explained by different charge states of O-atom vacancies and interstitials [2–4,8,9]. However, these defects are *better explained* by sub-oxide bonding arrangements that are clustered at nano-crystalline grain boundaries [10]. Pre-existing valence band and conduction band edge discrete defects have been reduced by (i) limiting the size of nano-crystalline grains to <2 nm [5], (ii) introducing N into HfO_2 [5], and (iii) depositing stable non-crystalline (Ti, Zr, Hf) Si oxynitrides.

2. Experimental

Thin films have been prepared by remote plasma-assisted chemical vapor deposition (RPECVD), reactive evaporation in an ultra-high vacuum (UHV) compatible system, and atomic layer deposition (ALD). Soft X-ray photoelectron spectroscopy (SXPS on beam-line U4A at the National Synchrotron Light Source), near edge X-ray absorption spectroscopy (NEXAS on beam line 10-1 at the Stanford Synchrotron Research Laboratory), vacuum

* Corresponding author. Tel.: +1 919 515 3301; fax: +1 919 859 3191.
E-mail address: lucovsky@ncsu.edu (G. Lucovsky).

0039-6028/$ - see front matter © 2007 Elsevier B.V. All rights reserved.
doi:10.1016/j.susc.2007.04.197

ultra-violet spectroscopic ellipsometry (VUV SE), and vacuum ultra-violet photoemission spectroscopy (UPS) studies have been performed on nano-crystalline transition metal (TM) elemental oxides: TiO_2, ZrO_2, and HfO_2 [4]. Analysis of these spectra provide crystal field (C-F) *average* energy differences between doubly degenerate $nd_{3/2}$ and triply degenerate $nd_{5/2}$ d-states ($n = 3$, 4 and 5) as in undistorted octahedral or tetrahedral arrangements. The spectra display additional d-state splittings associated with Jahn–Teller (J–T) d-state degeneracy removal from *cooperative distortions* from these symmetric bonding environments. These J–T distortions are particularly important π-bonding between TM and oxygen atoms, and are not present in the same TM sulfides or selenides. Studies performed on nano-crystalline TiO_2 have demonstrated that relative energies of conduction band J–T split d-state features in NEXAS O K_1 spectra, and in epsilon 2, ε_2, spectra from SE measurements are the same within an experimental uncertainty of ±0.15 eV. As shown in Fig. 1, average C-F splittings scale monotonically with the number of O-atom neighbors to the TM atoms in both nano- and noncrystalline TM oxides, silicates and Si oxynitrides. This scaling, and the correspondence between average C-F and J–T splittings in O K_1 and ε_2 d-state features in Fig. 2 provide the basis for using O K_1 spectra to identifying σ- and π-bonded conduction band d-states in nano-crystalline TM elemental oxides [10,11].

3. Spectroscopic results

Fig. 3a presents the SXPS valence band spectrum for HfO_2 indicating two occupied defect states above the valence band edge. Fig. 3b displays the VUV SE absorption edge spectrum, α, for HfO_2, displaying two defect states

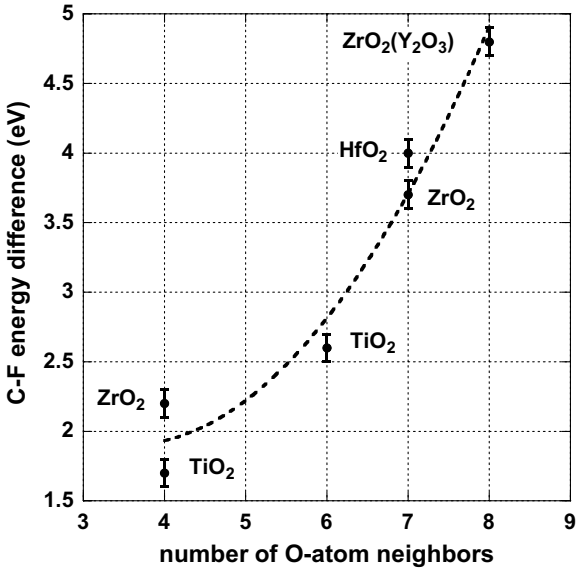

Fig. 1. Average C-F energy differences determined from NEXAS O K_1 spectra as a function the number of O-atom ligands for group IVB TM oxides.

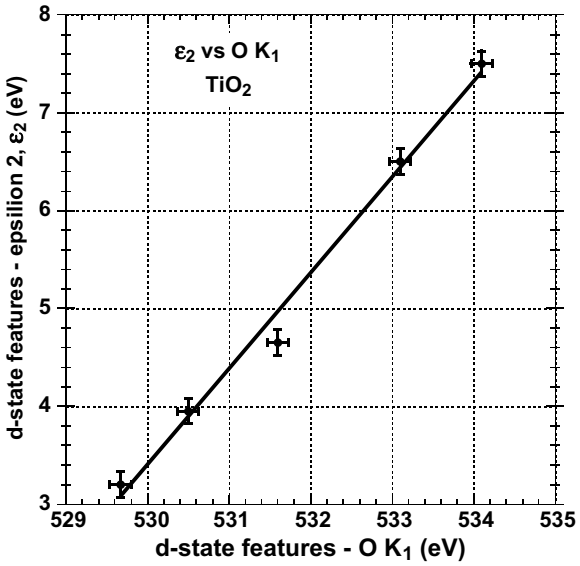

Fig. 2. Photon energies of Ti d-state features for ε_2 versus d-state features in O K_1 spectra.

~1–3 eV below the conduction band edge [2–4]. The α spectra contain d-state features at approximately the same relative energies as the ε_2 spectra, and equally important, the energy differences between these d-state features in the two spectra are the same within an experimental uncertainty of less than ±0.2 eV. These spectral features have been used to create the electron energy level diagram for $Hf(Zr)O_2$ in Fig. 4a. Photoconductivity and cathodo-luminescence spectra support the intrinsic character of the band edge defect states [2]. Fig. 4b is an energy level diagram from vis–VUV ε_2 conduction band, and SXPS valence band spectra for TiO_2 [2].

4. Defect state assignments

Several proposals have been made the microscopic origin of the electron and hole traps in ZrO_2 and HfO_2. Defect states have been addressed in Refs. [1–9] and [12] where a distinction is made between (i) *pre-existing defects*, those occurring in as-deposited and thermally annealed films, and (ii) *stress-induced defects*, those resulting from accelerated electrical stress [12]. The initial calculations for pre-existing defects were by the Robertson and Shluger groups [8,9], who focused on defect states within the forbidden energy gap associated with different charge states O-atom vacancies and O-atom/O_2 molecule interstitials [8,9]. These calculations are based on different local bonding: (i) the ideal CaF_2 structure by the Robertson group [8], and (ii) the experimentally determined $Hf(Zr)O_2$ monoclinic structure by the Shluger group [9]. Even though Hf(Zr) atoms are seven-fold coordinated in the monoclinic phase, and eight-fold coordinated in CaF_2, in both calculations, O-atom vacancy states are in the upper half of band gap, whilst O-atom/O_2 interstitial states are in the lower half of the band gap.

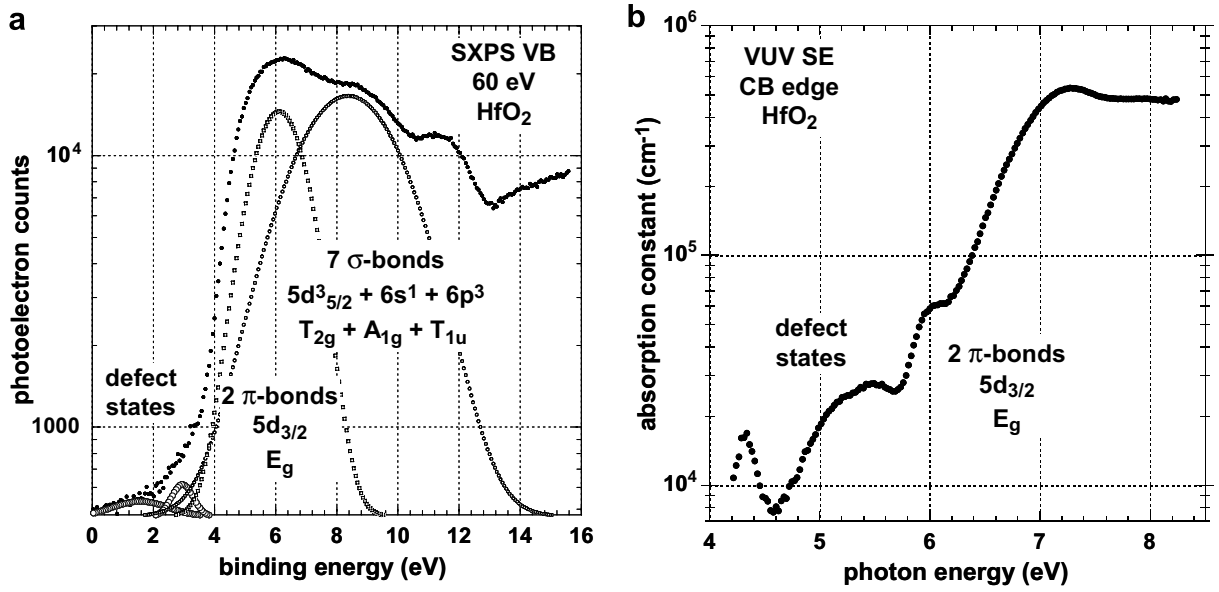

Fig. 3. (a) SXPS VB and (b) Vis–VUV SE absorption spectra for HfO_2.

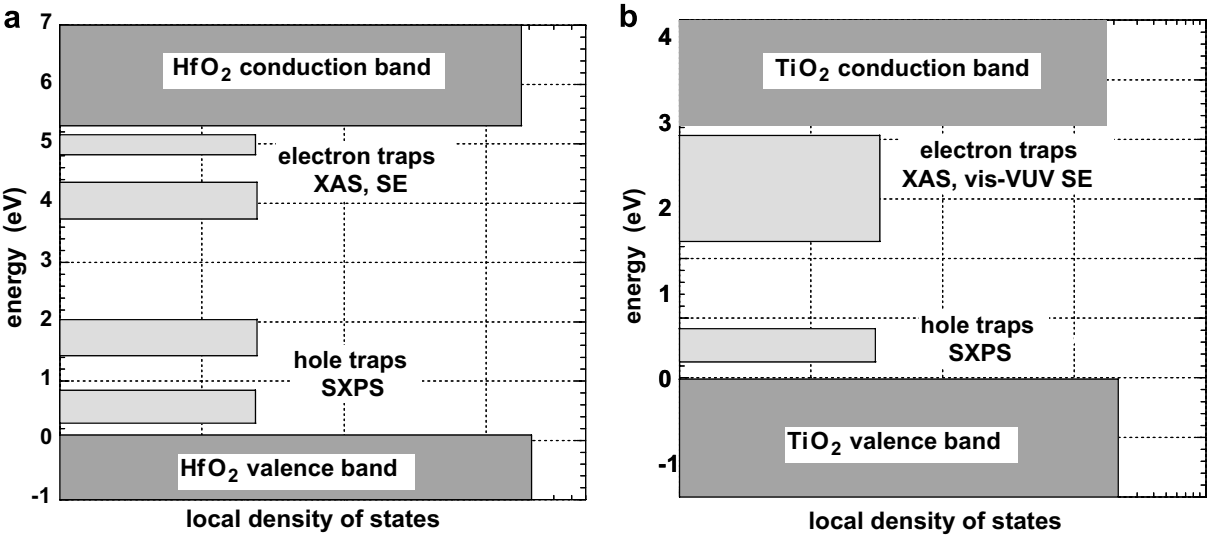

Fig. 4. Band edge and pre-existing defects from spectroscopic studies for (a) HfO_2 and (b) TiO_2.

In each of these calculations [8,9], the trapping-transport state below the conduction band edge is assigned to an empty O-atom vacancy [1,4]. The two conduction band edge spectral features in HfO_2 and ZrO_2 in the respective ε_2 and absorption, α, spectra are assigned to transitions from the valence band edge to unoccupied O-vacancies. These defects are, respectively, (i) ~0.5 eV below the band edge and (ii) ~1.8 to 2 eV below the spectral peak of the lowest d-state E_g conduction band feature. The cathodeluminescence (CLS) feature in HfO_2 at ~4.2 eV is assigned to a transition from the deeper O-atom vacancy state to the valence band edge, where the recombination is with electron beam generated holes [2–4]. Occupied defect states above the valence band edge are assigned to O/O_2 interstitials and contribute to hole trapping [1].

There are several significant issues with these calculations. The calculations in Refs. [8,9] used TM d-states constructed from orthogonalized plane wave basis states. This approach is valid for itinerant O 2s, and either Zr 5s and 5p, or Hf 6s and 6p states because of sufficiently rapid convergence; however, convergence may be too slow for the TM 3d, 4d and 5d states of this paper [13]. This issue has been addressed for NiO in a 1974 paper of Koiller and Falicov [13], who point out that atomic TM d-states should used in the basis set, rather than orthogonalized plane waves. In a recent publication, Gavartin and coworkers [14], used an atomic d-state basis, and their results for HfO_2 are now compared with the Xiong et al. paper from the Robertson group in which a plane wave d-state basis was used [8].

The primary difference between these calculations is that occupied states for the neutral and negatively charged O-atom vacancies are just below mid-gap for the atomic d-state calculation in Ref. [14], and about 1 eV higher in the gap in Ref. [8]. More importantly in neither of these calculations are there occupied O-vacancy states within 2 eV of the valence band edge. Occupied states are expected to be found ~4 eV above the valence band, and this is not the case. Thus even if calculations for O-atom vacancies employ TM atomic d-states, they do not describe the SXPS valence band edge defects for HfO_2 in Fig. 4a, or ZrO_2 as well. Based on Refs. [8] and/or [13], defects associated with both O-atom interstitials and O-vacancies are then required to account for the spectral results, but this cannot account for the absence of an addition SXPS feature ~4 eV above the valence band edge. In addition, to account for the four spectral features in Fig. 4a, it may be necessary to include more than one charge state of the vacancy and interstitial defects. Any combinations would be subject to a condition of charge neutrality. Considering the high densities of defects deduced from both spectroscopic and electrical measurements, vacancy–interstitial recombination must be addressed.

A second model, proposed in Ref. [2] for the high densities of pre-existing defects, $\sim 10^{12}\,cm^{-2}$ or $\sim 10^{18}\,cm^{-3}$ to defects attribute them to defect bonding arrangements clustered on grain-boundaries of nano-crystalline oxygen-deficient TM oxides. The grain-boundary model is supported by SE studies of the Berkeley group which show that defect state spectral features decrease with increasing annealing temperature [15], consistent with increases in crystallite size as a function of increasing post-deposition annealing temperatures.

A microscopic model for the grain-boundary model is first proposed for TiO_2, and then extended to HfO_2 and ZrO_2. Even though spectroscopic data for TiO_2 are qualitatively similar to data for HfO_2 and ZrO_2, the relative energies of defect features in the respective forbidden band gaps in Fig. 4a for HfO_2 and Fig. 4b for TiO_2 are quantitatively different. For HfO_2, the higher lying occupied state is <2 eV above the top of the valence band edge, and the lowest defect state in the upper half of the gap is ~4 eV above the valence band edge. In contrast, for TiO_2, the higher lying valence band edge state and broad defect feature below the conduction band edge are at approximately the same energy, 2.5 ± 0.15 eV above the valence band edge. The broad feature in the ε_2 spectrum for TiO_2 with a peak $\sim 2.6 \pm 0.15$ eV is essentially the same as the charge-transfer intra-d-state absorption of Ti^{3+} in the $Ti(H_2O)_6^{3+}$ complex, and in Ti_2O_3 [12,16,17]. This suggests that intrinsic defects in TiO_2 can be assigned to Ti ions a *formal charge* of 3+, i.e., Ti^{3+}. In the grain boundary model, these Ti^{3+} states are clustered at grain boundaries with a Ti_2O_3 average composition, or equivalently an O-atom deficient stoichiometry with respect to TiO_2. Based on the electronic structure for $Ti(H_2O)_6^{3+}$, the ground state for Ti^{3+} is a non-bonding T_{2g} state, and the higher lying state is an anti-bonding E_g state [16]. The energy difference between these states is approximately equal to average crystal field splitting of Ti in TiO_2 [16,17], and is 2.6 ± 0.1 eV as shown in Fig. 1.

A similar model is proposed for valence and conduction band edge *paired defects* in Fig. 4a for HfO_2. The average C-F splittings in the O K_1 edge spectra of monoclinic nanocrystalline HfO_2 is equal to 3.9 ± 0.15 eV. The *average energy separation* between the conduction and valence band edge defects in HfO_2 in Fig. 4a is 3.6 ± 0.2 eV, approximately the same as the C-F splitting in the O K_1 spectrum. A similar energy level diagram constructed for ZrO_2 (not shown) also yields approximately an average energy separation of 3.6 ± 0.2 eV. These comparisons for *pre-existing* defects in HfO_2 and ZrO_2, give additional support to the Hf^{3+} and Zr^{3+} bonding model for sub-oxide/O-deficient bonding arrangements grain boundary model. For HfO_2 and ZrO_2 these defect states, as well as the conduction band edge E_g states, display spectroscopically resolved J–T term splittings.

This model can be quantified by describing O-deficient $TiO_{2-\delta}$ and $HfO_{2-\delta}$ as mixtures of Ti_2O_3 and Hf_2O_3, and TiO_2 and HfO_2, respectively. If δ is the maximum concentration of defects, $\sim 10^{18}\,cm^{-3}$, or ~0.00003, then, $HfO_{2-\delta} = (1-2\delta)HfO_2 + 2\delta\ Hf_2O_3$, yielding an oxygen deficiency of ≈0.006% for $HFO_{2-\delta}$. Similar oxygen deficiencies are estimated for TiO_2 and ZrO_2. Estimating the density of defects from the relative absorption or photoemission in XAS and SE, or SXPS spectra gives a much higher apparent fraction of O-atom vacancies. This is addressed in the note added in proof at the end of this paper.

5. Discussion

HfO_2-based dielectrics display densities of reduced pre-existing defects in (i) ultra-thin (<2 nm) nano-crystalline HfO_2, and (ii) high HfO_2 content (~80%) phase separated Hf silicates [5,12]. XAS spectra are given in Fig. 5a and b. In Fig. 5a there is no detectable J–T splitting of the Hf E_g state, whilst J–T splittings are clearly evident in the 3 nm and 4 nm thick films. Similar results have been obtained for ZrO_2 films.

The band edge Hf E_g J–T splitting is also not observed in phase-separated Hf silicate films in Fig. 5a that are 2 nm, 3 nm and 4 nm thick. An increase in the relative amplitude of this E_g feature in 3 and 4 nm thick films is consistent with anisotropic grain grown, i.e., a larger crystallite size in the direction of the film growth. Similar results have been obtained for phase separated Zr silicate films.

There are two contributions to the reduced grain size: (i) total film thickness for the ultra-thin HfO_2 films in Fig. 5a, and (ii) inclusion of non-crystalline SiO_2 as a second phase in the Hf silicates in Fig. 5b with an 80% HfO_2 content.

A valence band edge defect that can be fit with two Guassians is observable in Fig. 6a as a distinct shoulder in the 4 nm thick HfO_2 film, whilst for a 2 nm film, there

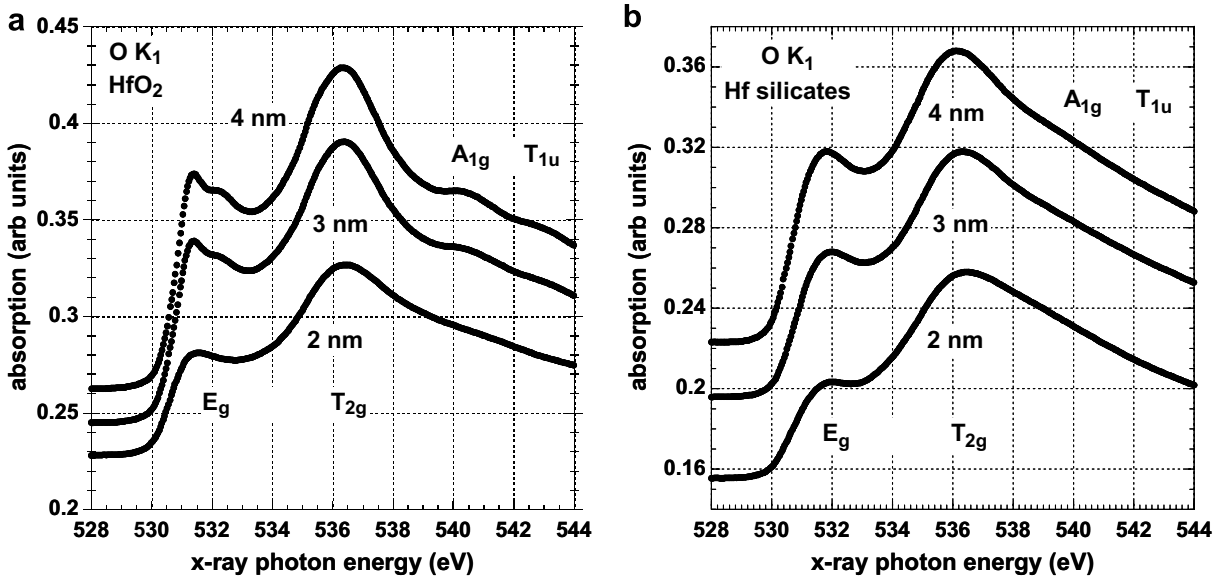

Fig. 5. O K_1 spectra for 2, 3 and 4 nm films: (a) HfO_2, and (b) phase-separated Hf silicates.

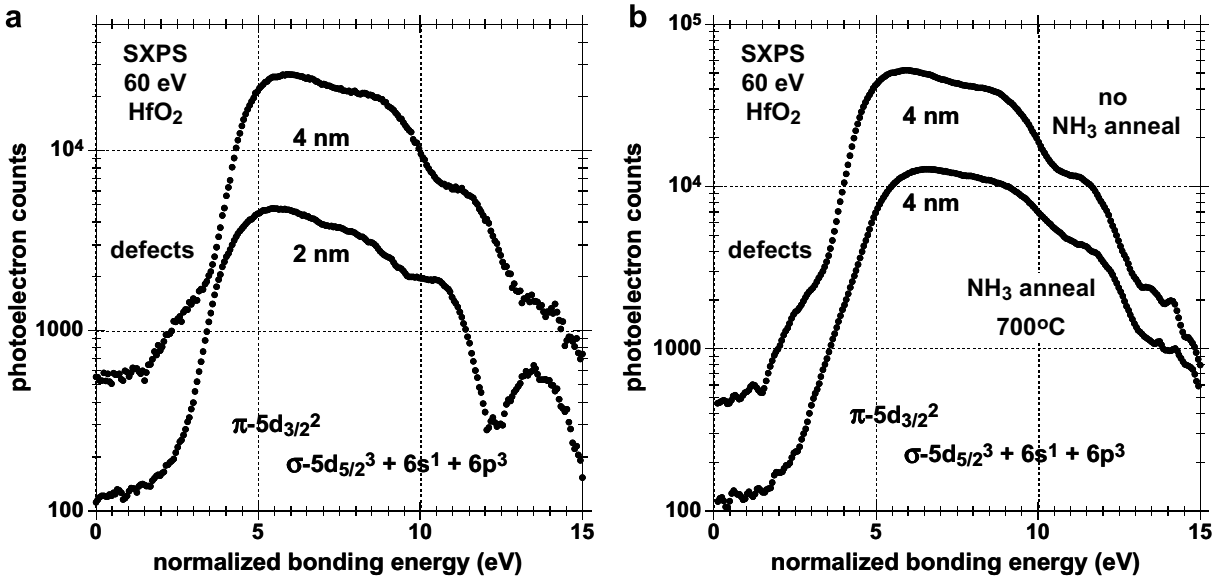

Fig. 6. SXPS VB spectra for (a) 2 and 4 nm thick HfO_2, and (b) 4 nm thick HfO_2 without (top), and with (bottom) N-incorporation from a 700 °C NH_3 post-deposition anneal.

is not a similar *distinct* shoulder, but instead a weaker band-edge feature tailing into the gap and corresponding to an approximately ten-fold reduction in the defect state density.

An additional approach for changing the character of the band edge defects in HfO_2 involves post deposition annealing in NH_3 at a temperature of 700 °C [5,12]. Films annealed in N_2 show no spectroscopic evidence for N-incorporation in N K_1 NEXAS spectra, whilst the films annealed in NH_3 indicate Hf–N bonding through the Hf d-state features. Fig. 6 compares SXPS valence band spectra of 4 nm thick HfO_2 films annealed in N_2 and NH_3 at 700 °C. The spectrum in Fig. 6b for the HfO_2 film with no Hf–N bonding indicates a spectrally-resolved band shoulder defect essentially the same as in Fig. 6a, whilst, the film annealed in NH_3 in Fig. 6b with Hf–N bonding instead displays a band edge tail that is significantly *softer* than for the 2.0 nm film in Fig. 6a. This softer edge is attributed to band tail defects similar to those in a-Si [18].

The results for defect reduction for the 2 nm film in Fig. 6a, and for the softer band edge in Fig. 6b for the film with Hf–N bonds are attributed to the same microscopic mechanism; a length scale of ~3 nm for coherent π-bonding interactions. In 4 nm thick films with no Hf–N bonding in Fig. 6a and b, the J–T split valence band edge intrinsic and defect states are each associated with d-state π-bonding

and require a length scale of order of >3 nm. The 2 nm thick film in Fig. 6a is *too thin* to support nano-crystalline grains >3 nm, and therefore J–T split states and shoulder defects are suppressed. For the 4 nm thick film in Fig. 6b with Hf–N bonding, interactions between π-bonding molecular orbitals on different pairs of Hf-atoms with both O- and N-neighbors are statistical, eliminating coherent π-bonding and giving rise to increased band-tailing rather than discrete defects. This length scale explanation is supported by model calculations in Ref. [19].

Equivalent oxide thicknesses (EOTs) as small as ~0.8 nm have been obtained for the ultra-thin HfO_2 and chemically-phase separated silicates [5,12]. The ultra-thin HfO_2 and chemically-phase separated Hf silicates also display reduced trapping, consistent with spectroscopic changes in valence band edge SXPS spectra. Similar results, but with EOTs ~1 nm, have been obtained for Zr and Hf Si oxynitride alloy devices with ~40% Si_3N_4, and approximately equal concentrations of SiO_2 and Zr or Hf oxide [20–22].

Note added in proof

Based on differences in absorption constant alone, the density of electrons in these band edge defect states would be at least ~0.5 to more than 1–3% of the occupied density of valence states, and at least 50 to 100 times larger than defect state densities determined from electrical measurements [1]. This difference is explained by noting that matrix elements for spatially-localized defect/dopant states in Si, Ge and III–V semiconductors are larger by one to two orders of magnitude than those for direct valence to conduction band transitions. This difference can be estimated by applying the *f*-sum rule that relates the integrated absorption to number of electrons in the initial state(s) of the transition [23]. The effective density of valence band atomic states in III–V direct band gap semiconductors is *determined or counted* by absorption that extends from the band edge, ~1.5 eV for GaAs to >30 eV, whereas band edge defects ~$10^{18}/cm^3$ yield measurable and comparable absorption in a spectral range within 0.5 eV of the band gap at 1.4 eV [24]. The ratio of the effective spectral widths, ~60 for this example, is a manifestation of the matrix element enhancement factor determined by an application of the *f*-sum rule. This in turn reconciles the apparent differences between spectroscopic measurements of this paper for band edge defect states, and the electrical measurements addressed in Ref. [1]. It also indicates that the estimate of O-vacancies determined from electrical measurements can be converted in an effective densities of defects that are electrically-active as discussed in the last paragraph in Section 4.

Acknowledgement

This research has been supported in part by ONR, SRC, the SRC-Sematech FEP center.

References

[1] J.-L. Autron, D. Munteanu, M. Houssa, in: M. Houssa (Ed.), High-*k* Gate Dielectrics, Inst. of Physics, Bristol, 2004 (Chapter 3.4).
[2] G. Lucovsky et al., IEEE Trans. Dev. Mat. Reliab. 5 (2005) 65.
[3] G. Lucovsky, J. Lüning, in: Proceedings of ESSDERC 2005, Grenoble, France, 2005, p. 439.
[4] G. Lucovsky et al., Microelectron. Eng. (2005) 110, and Refs. therein.
[5] P.D. Kirsch, et al., in: Proceedings of ESSDERC 2005, Grenoble, France, 2005, p. 367.
[6] M. Houssa et al., Semicond. Sci. Technol. 16 (2001) 31.
[7] X. Zu, M. Houssa, S. DeGendt, M. Hyens, Appl. Phys. Lett. 80 (2001) 1975.
[8] K. Xiong, J. Robertson, S.J. Clark, Appl. Phys. Lett. 87 (2005) 1, and Refs. therein.
[9] A.S. Foster et al., Phys. Rev. B 64 (2001) 224108;
A.S. Foster et al., Phys. Rev. B 65 (2002) 174117.
[10] F.A. Cotton, Chemical Applications of Group Theory, second ed., Wiley Interscience, New York, 1963.
[11] P.A. Cox, Transition Metal Oxides, Clarendon, Oxford, 1992.
[12] J.L. Gavartin et al., J. Appl. Phys. 97 (2005) 053704.
[13] B. Koiller, L.M. Falicov, J. Phys. C: Solid State Phys. 7 (1974) 299.
[14] J.L. Gavartin et al., Appl. Phys. Lett. 89 (2006) 082908.
[15] T.-J.H. Takeuchi, H. Daewon, King, J. Vac. Sci. Technol. A22 (2004) 1337.
[16] H.B. Gray, Electrons and Chemical Bonding, Benjamin, New York, 1965.
[17] C.J. Ballhausen, H.B. Gray, Molecular Orbital Theory, Benjamin, New York, 1964.
[18] M.J. Williams, S.M. Cho, S.S. He, G. Lucovsky, J. Non-Cryst. Solids 164/166 (1993) 67.
[19] R.A. Wheeler et al., J. Am. Chem. Soc. 108 (1986) 2222.
[20] B. Ju, Properties of Zr–Si Oxynitride Dielectric Alloys, PhD. Thesis, NC State University, Raleigh USA, 2003.
[21] G. Lucovsky et al., Microelectron. Reliab. 46 (2006) 1623.
[22] S. Lee, G. Lucovsky, unpublished.
[23] H.R. Philipp, H. Ehrenreich, Phys. Rev. 129 (1963) 1550, and Refs. therein.
[24] G. Lucovsky, Appl. Phys. Lett. 5 (1964) 37.